Supporting Information: Unexpected trends in the enhanced Ce^{3+} surface concentration in ceria-zirconia solid solutions

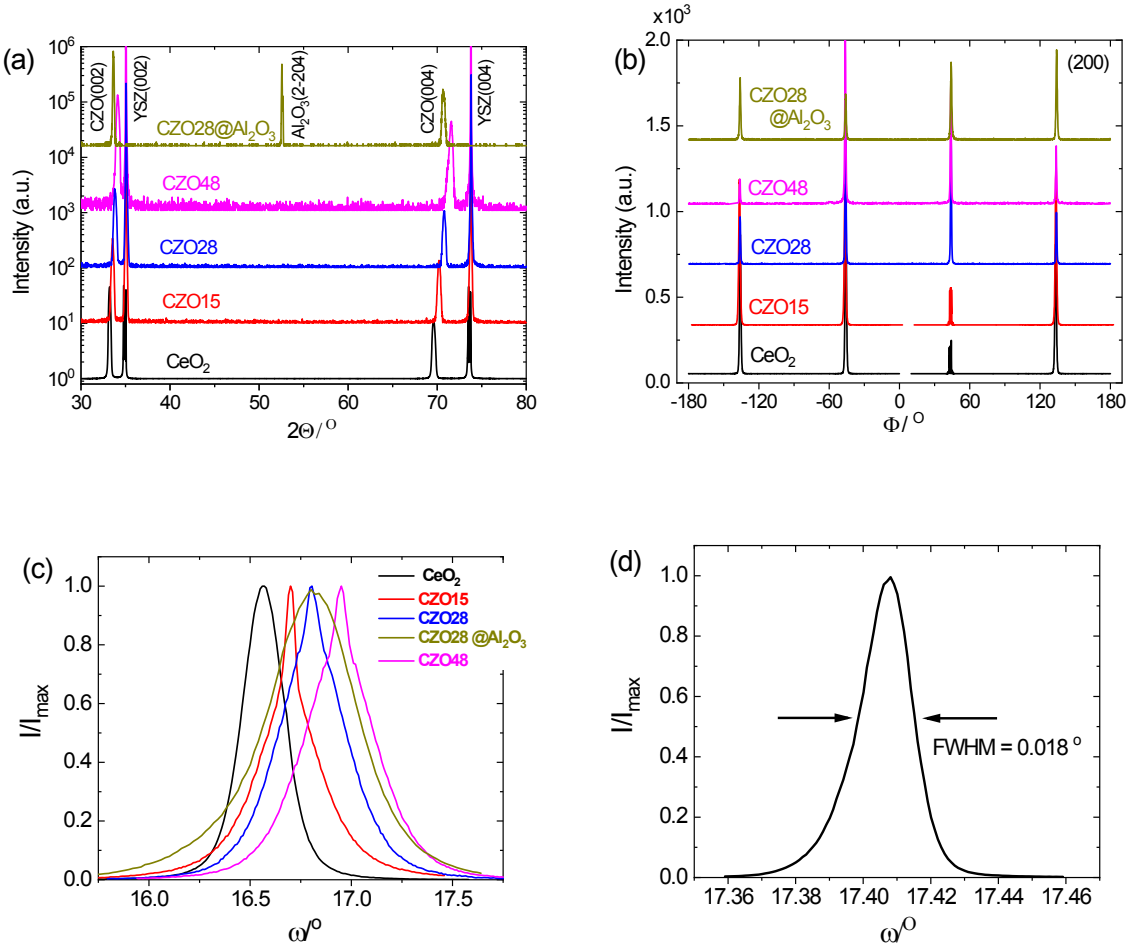

Figure S1. X-ray diffraction patterns of (a)-(c) CZOxx films (220 nm) on YSZ (001) and CZO28 film (490 nm) on r-plane Al_2O_3 as indicated, and of (d) YSZ (001) substrate: (a) Specular θ–2θ scans; (b) azimuthal ϕ scans; (c), (d) rocking curves about the CZO or YSZ (002) Bragg peak, the latter indicating instrument resolution for curves shown in (c). Data collected using a Cu kα X-ray source (50kV, 240mA). In (a) and (b) patterns for individual samples are offset along the intensity axis for clarity.

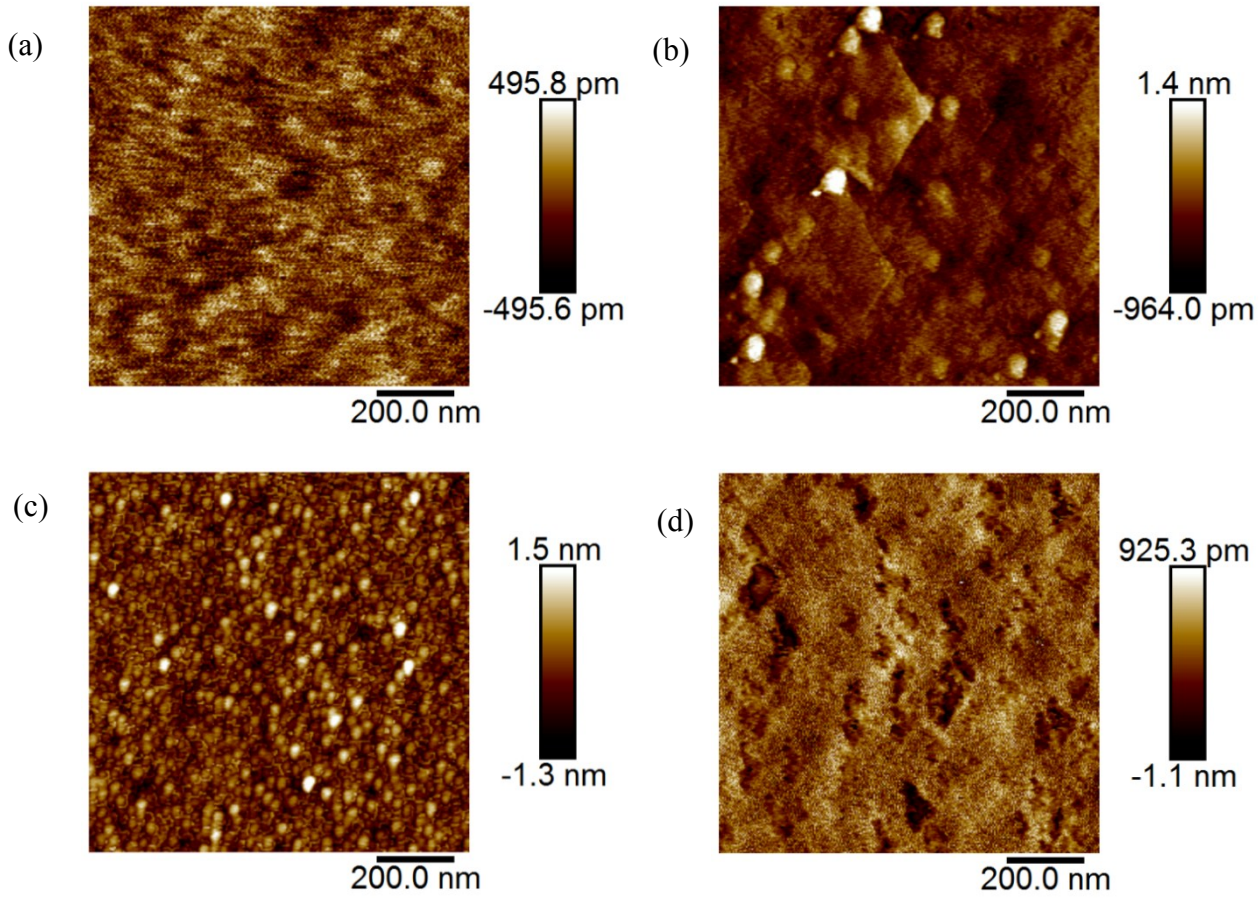

Figure S2. Surface topologies as measured by atomic force microscopy of CZOxx films on YSZ(001): (a) CeO_2; (b) CZO15; (c) CZO28; and (d) CZO48. Images collected using a Bruker Dimension FastScan in tapping mode.

Table S1. Crystallographic features of non-graded 220 nm CZOxx films (where xx is the mole % Zr) grown on YSZ (001) unless stated otherwise. Domain sizes (calculated using the Scherrer equation after accounting for instrument broadening[1]. For Zr bearing compositions grown on YSZ, two different domain sizes along the a axis were calculated from the presence of two overlapping peaks with two different FWHM values.

Sample/Material	Bulk a_0 (Å)	Mismatch vs substrate (%)	Rocking curve FWHM (°)	Domain size along a axis (nm)	Domain size along c axis (nm)	AFM rms surface roughness (nm)
CeO_2	5.4158(8)	5.3	0.25	35	150	0.14
CZO15	5.3723(8)[a]	4.3	0.045/0.21	190/39	110	0.31
CZO28	5.3288(6)	3.5	0.071/0.33	120/25	140	0.39
CZO48	5.273(5)	2.6	0.062/0.33	140/25	140	0.27
YSZ substrate	5.14105(2)[2]	--	0.018		--	
CZO25 (490 nm) on r-Al_2O_3	5.3288(6)	2.1 & 12.0[b]	0.51	14	59	0.43

[a)] interpolated from CeO_2 and CZO25 results as this composition was not directly prepared in bulk form.

[b)] the termination on the r-plane of Al_2O_3 presents a pseudo-cubic parallelogram cell shape with relevant orthogonal interatomic distances of 4.758 and 5.218 Å.[3]

The specular θ–2θ scans of the non-graded films showed, in addition to the peak shift to higher angle with increasing Zr doping, a broadening of the (00L) peaks, which diminished with Zr doping, Figure S1(a). Significant broadening in the rocking curve, particularly at low zirconium content, was also evident, Figure S1(c). In the case of the Zr-bearing compositions on YSZ, a sharp peak with breadth only slightly larger than that of the substrate, overlaps with the broad component. In a similar study of GDC on YSZ(111) Petrisor et al. attributed this type of profile to a combination of high quality epitaxy, producing the sharp feature, and a high concentration of misfit dislocations, producing the broad feature.[4] Here, the sharp feature suggests an in-plane domain size of a few hundred nm.

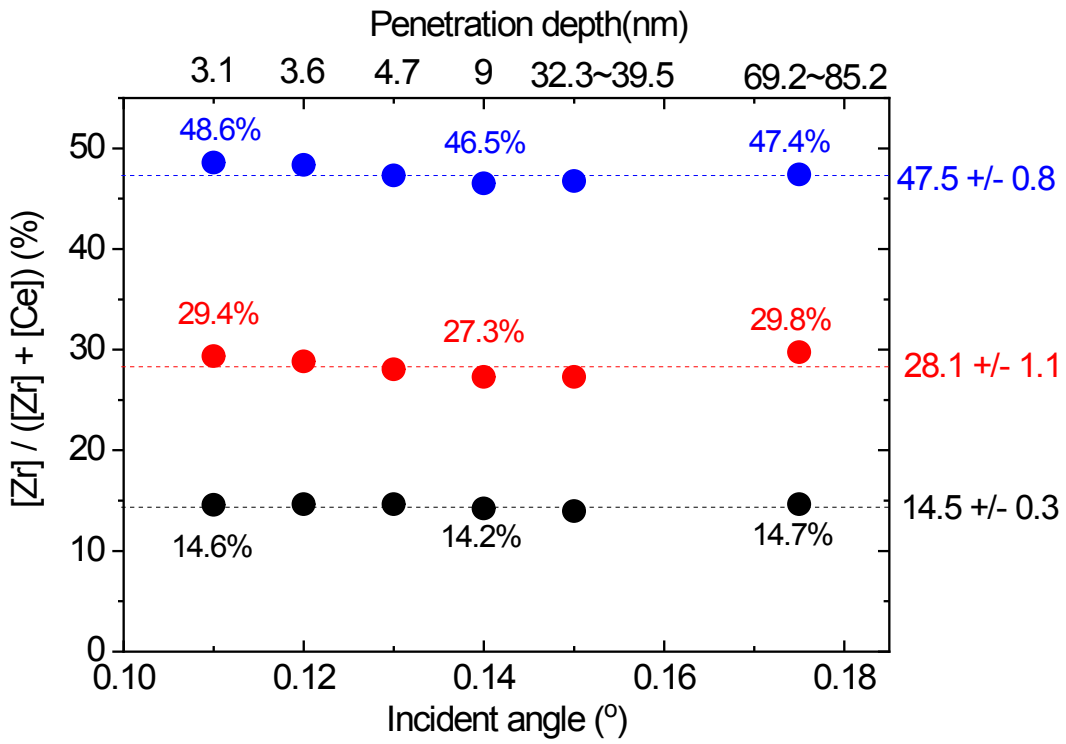

Figure S3 Angle resolved X-ray fluorescence chemical analysis of uniform composition CZOxx films (220 nm) on YSZ (100) with targeted compositions of: (top) $Ce_{0.55}Zr_{0.45}O_{2-\delta}$; (middle) $Ce_{0.75}Zr_{0.25}O_{2-\delta}$; (bottom) $Ce_{0.875}Zr_{0.125}O_{2-\delta}$. Based on these measurements, films are respectively denoted as CZO48, CZO28, and CZO15. The results reveal that the film composition is, in all cases, uniform along the thickness direction. The dramatic change in penetration depth near the 0.14° critical angle is due to the evanescent wave absorption effect.[5]

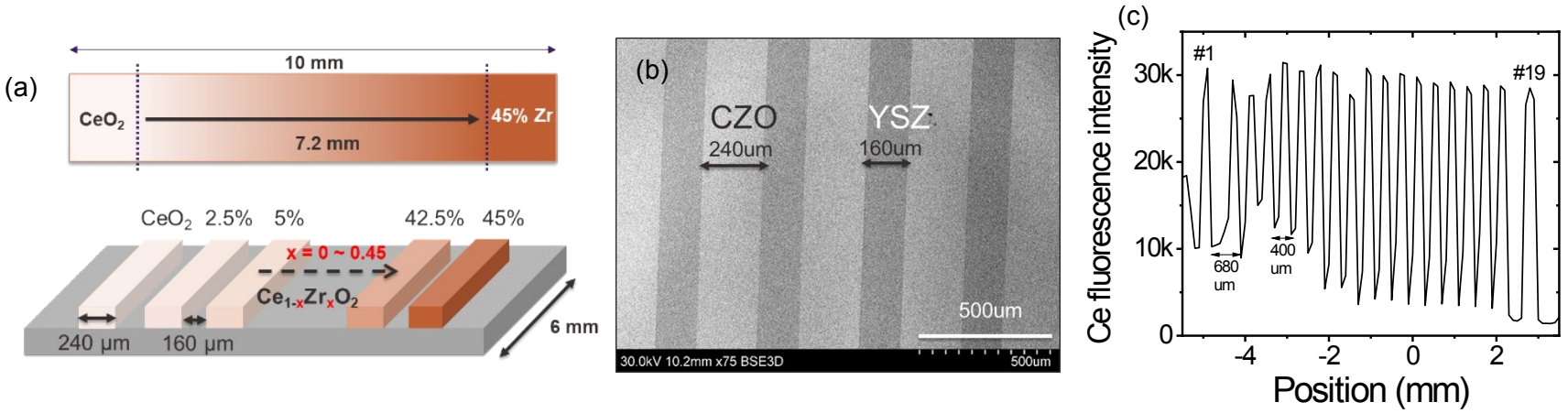

Figure S4. Patterning of compositionally graded CZO film grown on YSZ(001): (a) schematic of pattern layout; (b) scanning electron micrograph revealing CZO and YZO regions; and (c) variation of Ce fluorescence intensitiy as a function of position showing the presence of 19 strips. Due to beamtime constraints, 10 of these strips were studied by XANES. The end member composition CeO_2 was not captured in the gradient film and was accordingly studied (only) in the compositionally uniform geometry.

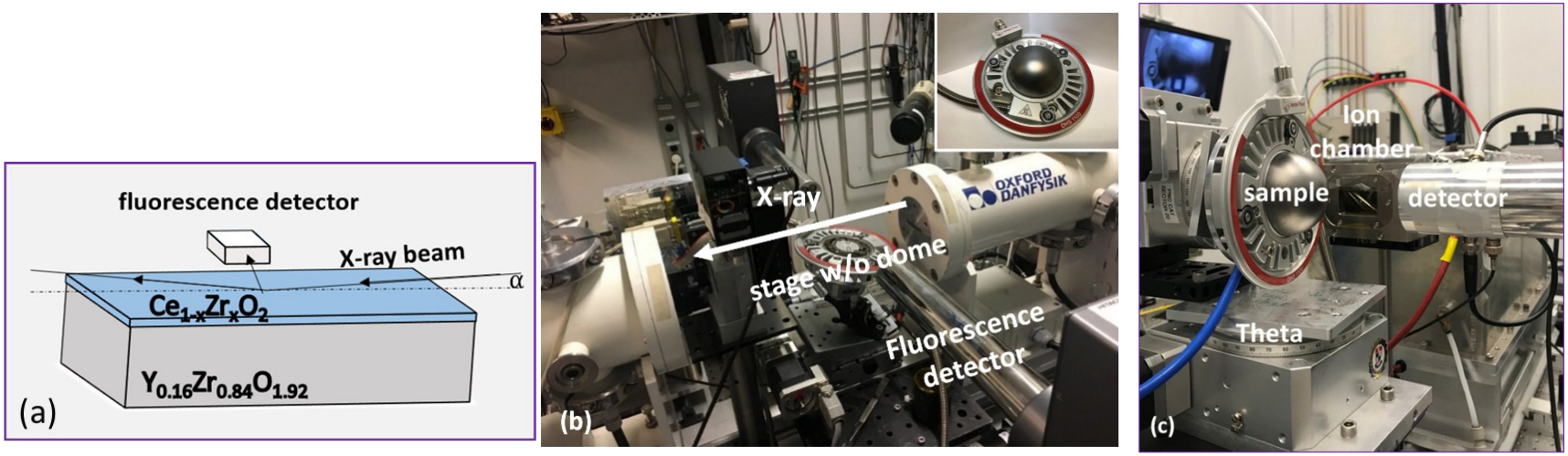

Figure S5. Experimental configuration for performing Ce L_3 edge XANES measurements from $Ce_{1-x}Zr_xO_{2-\delta}$ films (220 nm), grown on single crystal YSZ (001): (a) schematic of the beam-sample geometry (with only one detector shown for clarity), (b) photograph of the experimental setup at DND-CAT Sector 5 APS, with an inset showing the dome when closed for atmosphere control, and (c) photograph of the experimental setup at Sector 20 APS. For the actual measurement, the detectors are placed as close to the sample stage as possible (for example, by moving the detectors along the direction indicated in (b)) in order to maximize the signal.

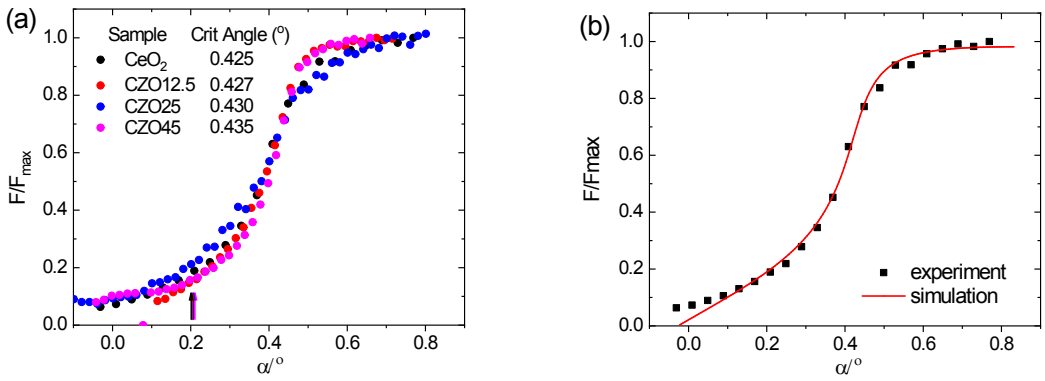

Figure S6. (a) Normalized Ce Lα fluorescence signal measured from non-graded CZO films as a function of incident angle α, using an incident photon energy of Eγ =5733 eV (obtained under ambient conditions). Each curve was aligned along the horizontal axis to match a relative intensity of 0.69 to the computed critical angle (reported in the inset). Arrows indicate angle of measurement for surface-sensitive experiments. (b) Comparison between measured and calculated fluorescence yields for CeO_2. The calculation is based on Fresnel theory for reflection and transmission[6] at a CeO_2 mirror surface. At the incident energy of E_γ = 5733 eV, the critical angle is 0.425°. (The calculation does not account for any surface roughness, nor for the fact that the beam subtends beyond the length of the sample for α < 0.29 °). The X-ray reflection signal from each film was recorded simultaneously with the fluorescence signal. A sharp increase in intensity on passing from above to below the critical angle was observed (not shown). Similar results were obtained from each position on the graded sample.

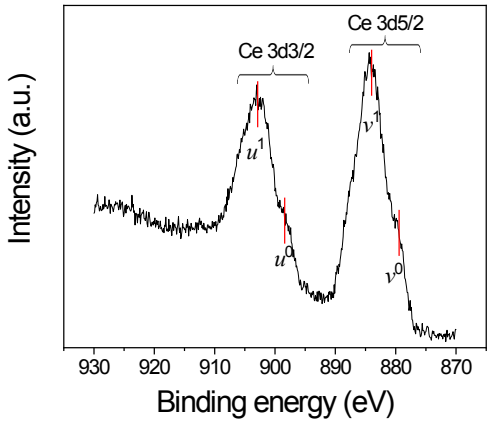

Figure S7. X-ray photoelectron spectroscopy (XPS) study of the $CeAlO_3$ film. The spectrum shows peaks only from Ce^{3+}; a peak at 918 eV would be indicative of the presence of Ce^{4+}.

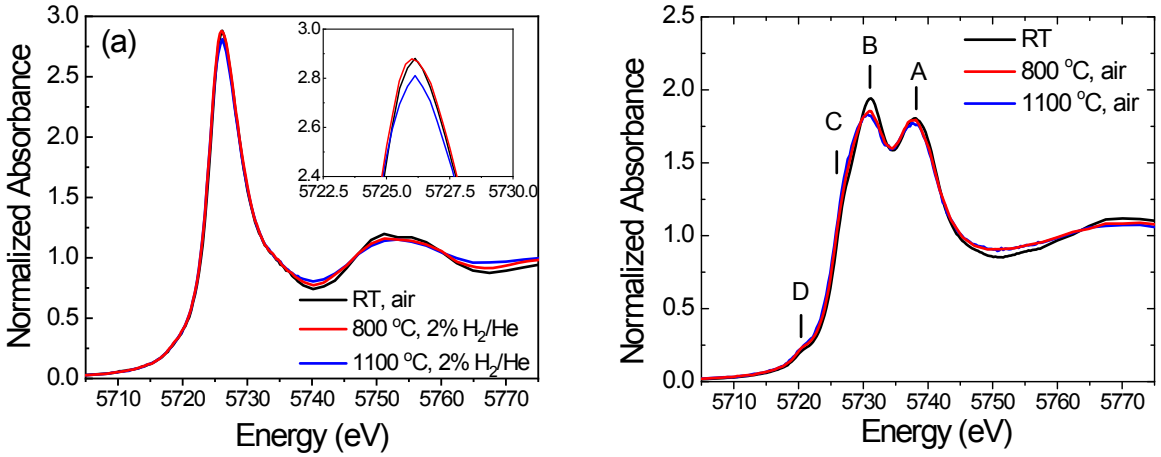

Figure S8. Ce L_3 edge XANES results collected at $\alpha = 10°$ at the conditions indicated from: (a) $CeAlO_3$ film showing peaks only from Ce^{3+}; and (b) CeO_2 showing only peaks from Ce^{4+}. In the case of $CeAlO_3$ high temperature spectra are collected under hydrogen to avoid any possibility of oxidation. Inset in (a) shows zoom in of the white line peak. The effects of thermal broadening are apparent in both sets of spectra. The results of Gaussian fitting of the four peaks in (b) for the three different measurement temperatures are summarized in Table S2.

Table S2. Gaussian fitting parameters for the four peaks in Figure S8(b), over the range (E_0-15, E_0+20) eV. Number in parenthesis is the uncertainty in the final digit(s).

		RT, air	800 °C, air	1100 °C, air
Peak D	Peak, position (eV)	5721(5)	5722(4)	5721(9)
	Peak, std (eV)	2.23(9)	2.39(11)	2.29(11)
	Peak, Area	0.5(4)	0.6 (5)	0.53(9)
Peak C	Peak, position (eV)	5727.00(16)	5726.8(3)	5727.0(3)
	Peak, std (eV)	1.14(4)	1.35(10)	1.25(8)
	Peak, Area	0.74(6)	0.74(17)	0.69(12)
Peak B	Peak, position (eV)	5730.76(5)	5730.47 (10)	5730.35(13)
	Peak, std (eV)	2.241(19)	2.48(6)	2.52(10)
	Peak, Area	5.79(13)	5.72(21)	5.6(3)
Peak A	Peak, position (eV)	5738.10(9)	5737.96(21)	5737.90(22)
	Peak, std (eV)	3.005(22)	2.98(4)	3.07(7)
	Peak, Area	6.84(13)	6.3(3)	6.3(3)
Arctan Step	Step, position (eV)	5724.5(7)	5724.8(8)	5724.3(13)
	Step, width (eV)	1.81(6)	1.96(7)	1.85(10)
	Step, height	0.939(14)	0.99(3)	0.98(3)

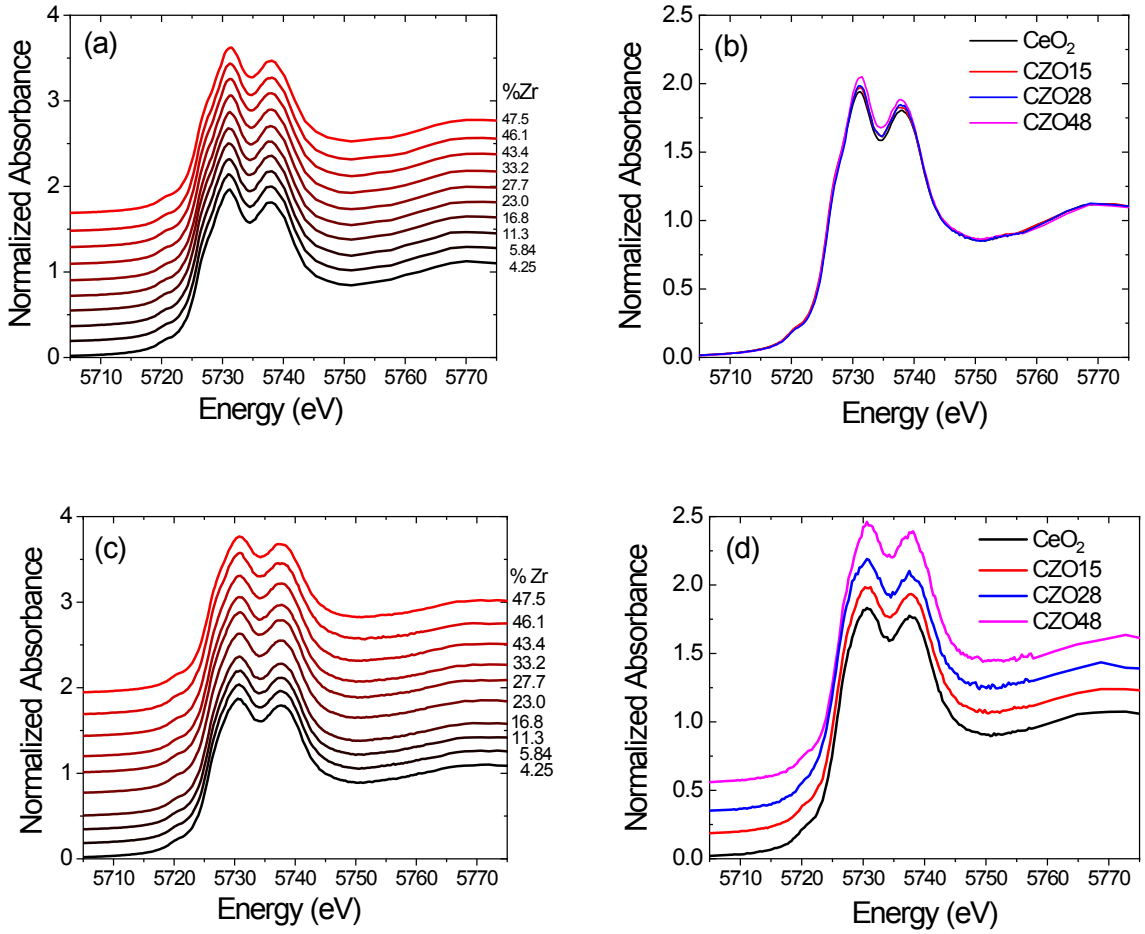

Figure S9. Bulk Ce L_3 edge XANES for ceria and CZOxx as measured under air at: (a), (b) at RT, (c) 800 °C, and (d) 1100 °C. Spectra in (a) and (c) collected from a single, compositionally graded film; and (c) and (d) are collected from four distinct, compositionally uniform films. Slight differences in spectra are evident (shown most clearly in (b)), despite the presence of Ce entirely in the 4+ oxidation state. These differences are presumably a result of second nearest neighbor effects and underscore the need to measure reference spectra using the Zr composition of interest. In (a), (c) and (d) spectra are offset for clarity. These spectra capture the impact of temperature and chemistry on the Ce^{4+} absorption behavior, and hence are used as the reference spectra for LCF analysis and quantification of Ce^{3+} concentration.

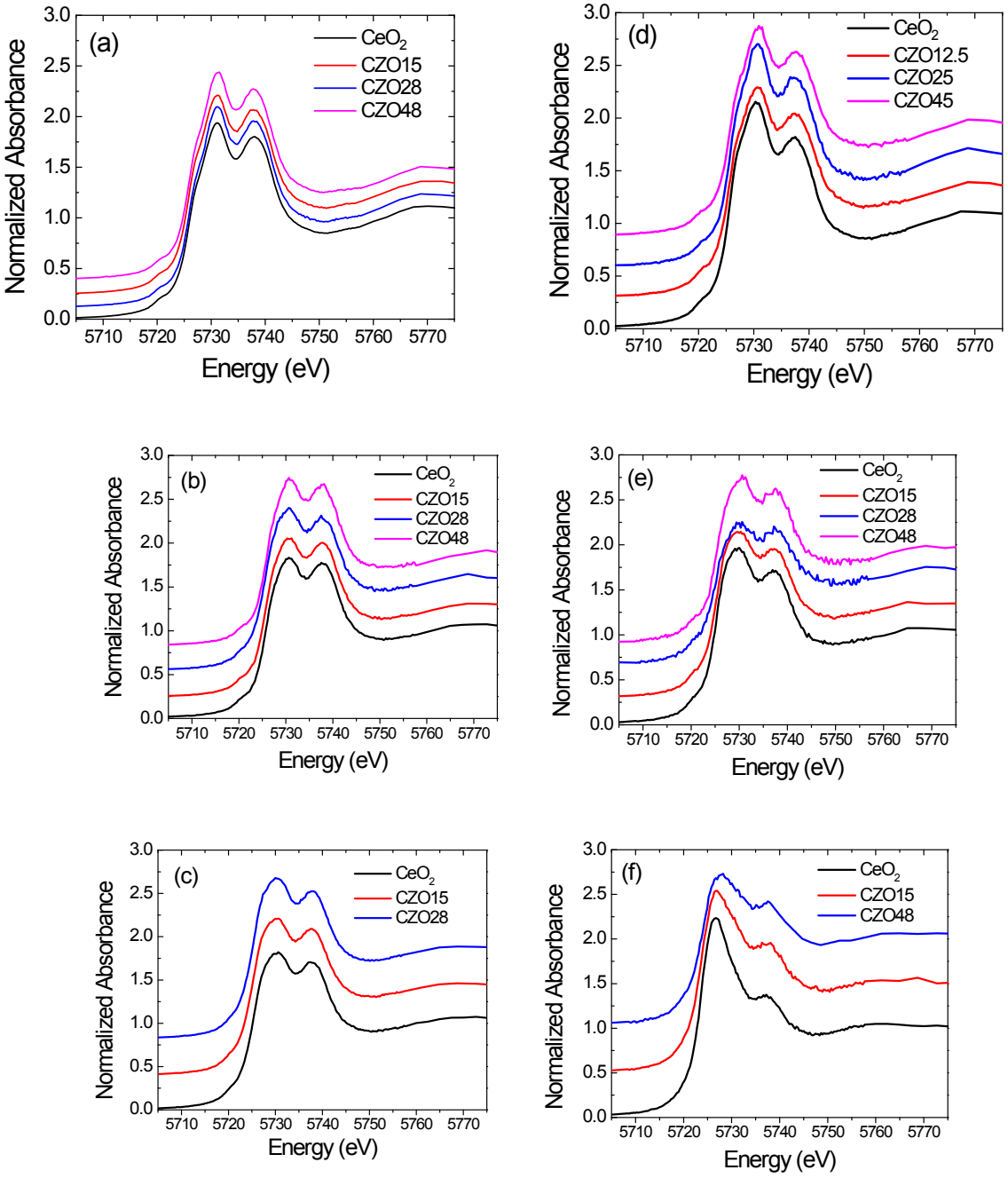

Figure S10 Ce L_3 edge XANES for ceria and CZOxx non-graded films: (a)-(c) bulk spectra and (d)-(f) surface spectra, with (a) (d) at RT, under air; (b) (e) at 1100 °C, under air; and (c) (f) at 1100 °C under vacuum ($pO_2 \sim 2.3$ mTorr). Measurement of CZO48 at 1100 °C under vacuum was unsuccessful due to loss of atmosphere control. Data in (a) and (b) are identical to those in Figure S9(d) and S9(d), respectively, and are duplicated here for ease of comparison.

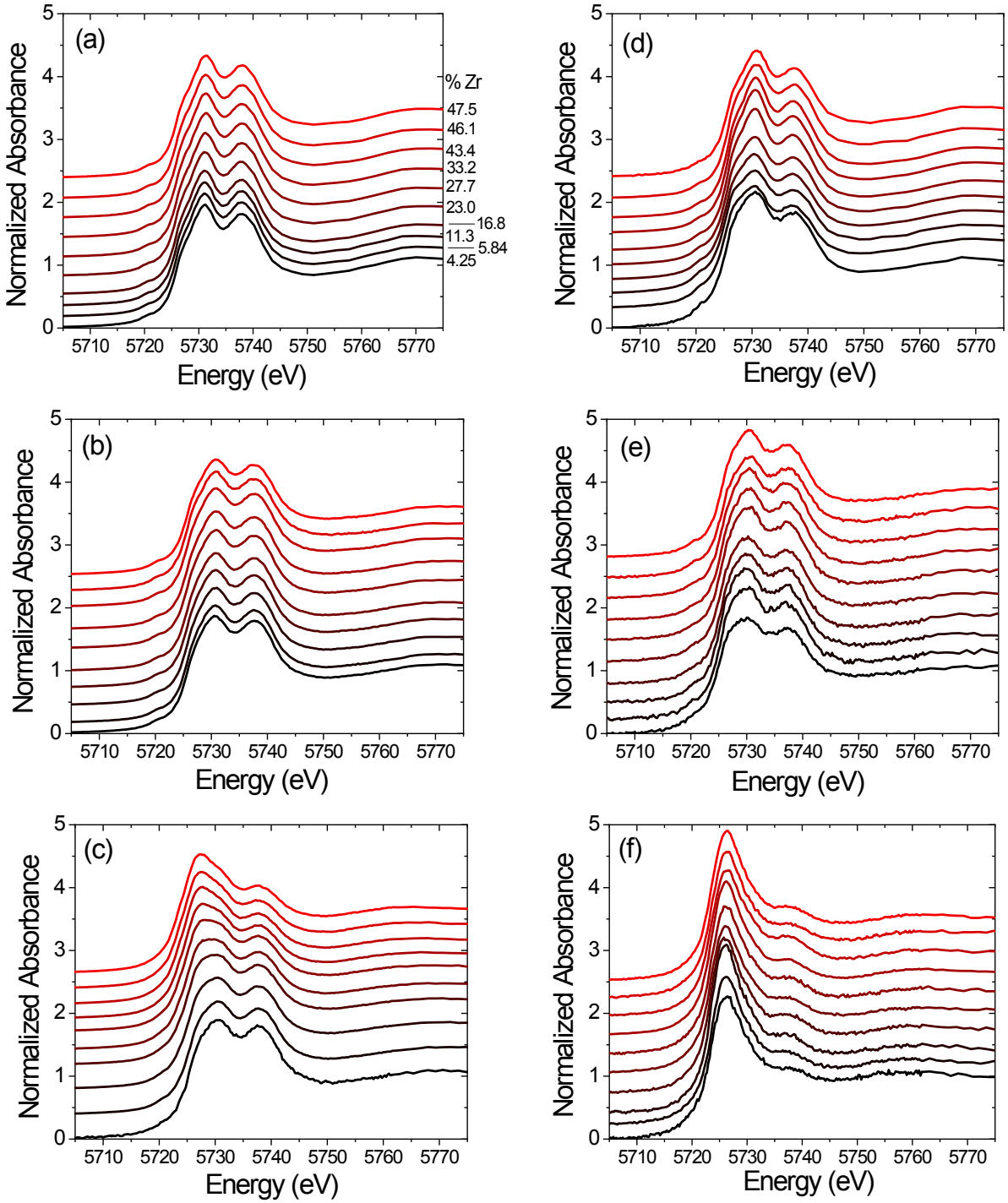

Figure S11 Ce L_3 edge XANES for CZOxx from the compositionally graded film: (a)-(c) bulk spectra and (d)-(f) surface spectra, with (a) (d) at RT, under air; (b) (e) at 800 °C, under air; and (c) (f) at 800 °C, under H_2/He ($pO_2 = 7.4 \times 10^{-14}$ mTorr). Legend information provided in (a) applies to all panels. Data in (a) and (b) are identical to those in Figure S9(a) and S9(c), respectively, and are duplicated here for ease of comparison.

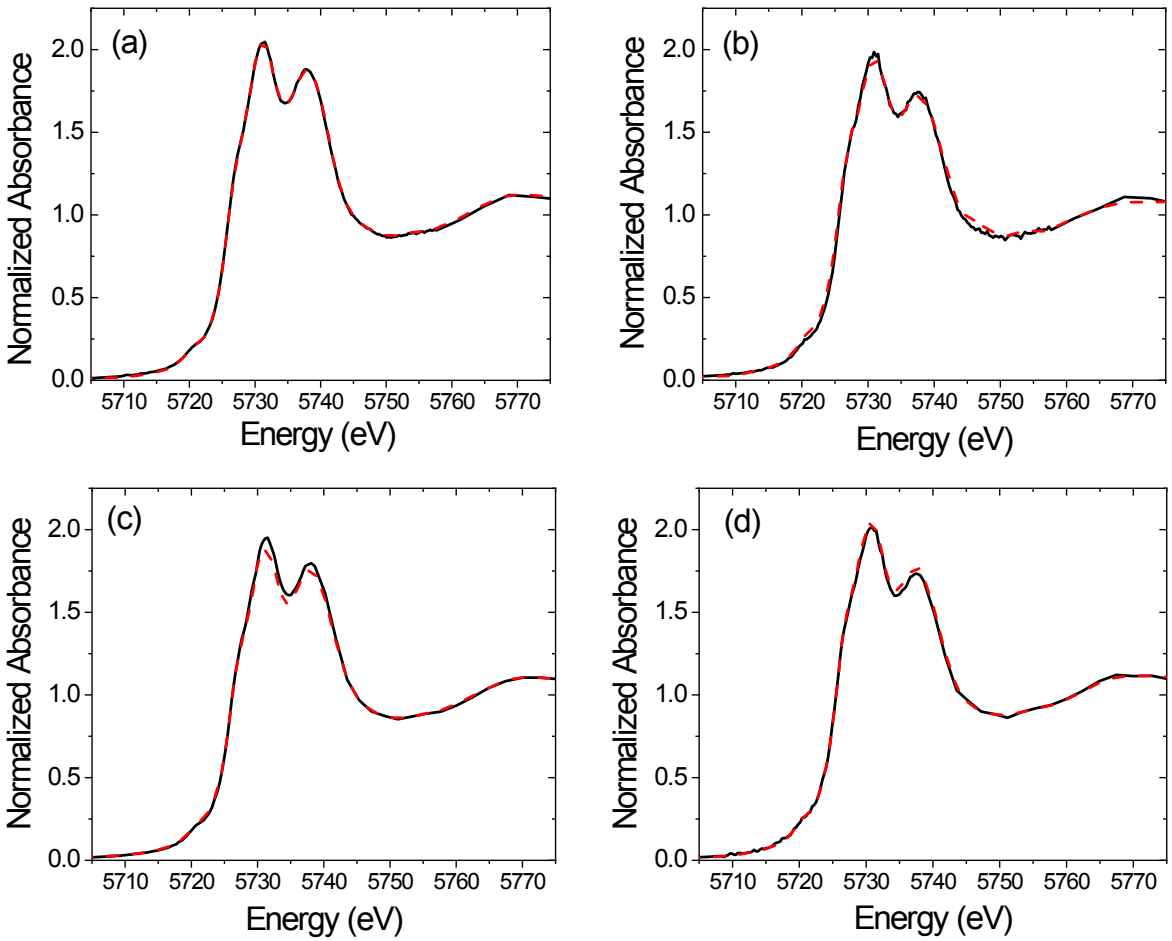

Figure S12. Normalized Ce L_3 edge XANES spectra of CZO48 taken from (a) bulk region (b) surface regions of the non-graded film, and (c) bulk region (d) surface region of the graded film, collected before (black line) and after (red dash line) the complete suite of XANES measurement, under air and ambient temperature. Results demonstrate that the film returns to the initial state upon completion of the measurements.

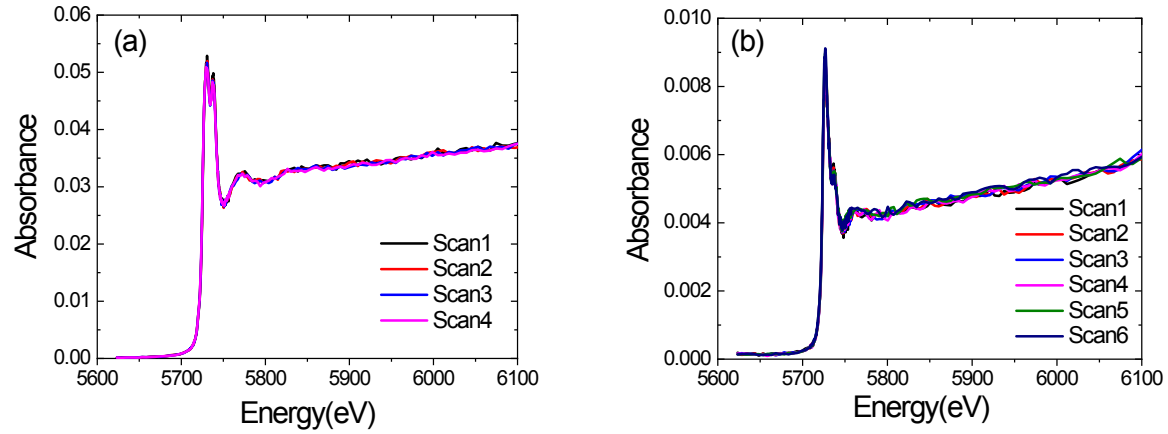

Figure S13. Sequential raw Ce L_3 edge XANES spectra of $CeO_{2-\delta}$ measured at 1100 ^{o}C under vacuum: (a) bulk region and (b) surface region. The measurement time for each spectrum was about 22 min. No evolution of spectra over the course of the measurement, 4 h in the case of (b), was detected, indicating that within this time scale, beam radiation damage is negligible.

References

1 Langford, J. I. & Wilson, A. J. C. Scherrer after 60 years - Survey and some new results in determination of crystallite size. *J. Appl. Crystallogr.* **11**, 102-113, doi:10.1107/s0021889878012844 (1978).

2 Itoh, T. *et al.* Effect of Annealing on Crystal and Local Structures of Doped Zirconia Using Experimental and Computational Methods. *The Journal of Physical Chemistry C* **119**, 8447-8458, doi:10.1021/jp5117118 (2015).

3 Bick, D. S. *et al.* (001) and (111) Single-Oriented Highly Epitaxial CeO2 Thin Films on r-Cut Sapphire Substrates. *J. Electron. Mater.* **44**, 2930-2938, doi:10.1007/s11664-015-3728-2 (2015).

4 Petrisor, T. *et al.* Ordered misfit dislocations in epitaxial Gd doped CeO_2 thin films deposited on (001)YSZ single crystal substrates. *Applied Surface Science* **433**, 668-673, doi:10.1016/j.apsusc.2017.09.202 (2018).

5 Becker, R. S., Golovchenko, J. A. & Patel, J. R. X-ray evanescent-wave absorption and emission. *Phys. Rev. Lett.* **50**, 153-156, doi:10.1103/PhysRevLett.50.153 (1983).

6 Parratt, L. G. Surface Studies of Solids by Total Reflection of X-rays. *Physical Review* **95**, 359-369, doi:10.1103/PhysRev.95.359 (1954).